*Protein Science* (1994), *3*:282–290. Cambridge University Press. Printed in the USA.


# Enzyme IIB$^{cellobiose}$ of the phosphoenol-pyruvate-dependent phosphotransferase system of *Escherichia coli*: Backbone assignment and secondary structure determined by three-dimensional NMR spectroscopy

EISO AB,[1] GEA K. SCHUURMAN-WOLTERS,[1] MILTON H. SAIER,[2] JONATHAN REIZER,[2] MICHEL JACUINOD,[3] PETER ROEPSTORFF,[3] KLAAS DIJKSTRA,[1] RUUD M. SCHEEK,[1] AND GEORGE T. ROBILLARD[1]

[1] The Groningen Biomolecular Science and Biotechnology Institute, University of Groningen, Nijenborgh 4, 9747 AG Groningen, The Netherlands
[2] Department of Biology, University of California at San Diego, La Jolla, California 92093-0116
[3] Department of Molecular Biology, Odense University, Campusvej 55, 5230 Odense M, Denmark

(RECEIVED November 10, 1993; ACCEPTED December 15, 1993)

**Abstract**

The assignment of backbone resonances and the secondary structure determination of the Cys 10 Ser mutant of enzyme IIB$^{cellobiose}$ of the *Escherichia coli* cellobiose-specific phosphoenol-pyruvate-dependent phosphotransferase system are presented. The backbone resonances were assigned using 4 triple resonance experiments, the HNCA and HN(CO)CA experiments, correlating backbone $^{1}H$, $^{15}N$, and $^{13}C\alpha$ resonances, and the HN(CA)CO and HNCO experiments, correlating backbone $^{1}H$,$^{15}N$ and $^{13}CO$ resonances. Heteronuclear $^{1}H$-NOE $^{1}H$-$^{15}N$ single quantum coherence ($^{15}N$-NOESY-HSQC) spectroscopy and heteronuclear $^{1}H$ total correlation $^{1}H$-$^{15}N$ single quantum coherence ($^{15}N$-TOCSY-HSQC) spectroscopy were used to resolve ambiguities arising from overlapping $^{13}C\alpha$ and $^{13}CO$ frequencies and to check the assignments from the triple resonance experiments. This procedure, together with a 3-dimensional $^{1}H\alpha$-$^{13}C\alpha$-$^{13}CO$ experiment (COCAH), yielded the assignment for all observed backbone resonances. The secondary structure was determined using information both from the deviation of observed $^{1}H\alpha$ and $^{13}C\alpha$ chemical shifts from their random coil values and $^{1}H$-NOE information from the $^{15}N$-NOESY-HSQC. These data show that enzyme IIB$^{cellobiose}$ consists of a 4-stranded parallel $\beta$-sheet and 5 $\alpha$-helices. In the wild-type enzyme IIB$^{cellobiose}$, the catalytic residue appears to be located at the end of a $\beta$-strand.

**Keywords:** cellobiose; NMR; phosphocysteine; phosphoenolpyruvate-dependent phosphotransferase system; protein structure determination; triple resonance

Enzyme IIB$^{cellobiose}$ is the catalytic domain of the phosphoenol-pyruvate-dependent cellobiose phosphotransferase system (Parker & Hall, 1990; Reizer et al., 1990). In this system, a phosphoryl group is transferred from phosphoenol-pyruvate via enzyme I, the histidine containing protein, and enzyme IIA$^{cel}$ to enzyme IIB$^{cel}$. Phospho-IIB$^{cel}$ donates its phosphoryl group to cellobiose after transport of this sugar through the membrane by enzyme IIC$^{cel}$. (For general reviews of the PEP-dependent PTS, see Meadow et al. [1990], Lolkema and Robillard [1992], Saier and Reizer [1992], and Postma et al. [1993].) The phosphorylation site of IIB$^{cel}$ is most likely Cys 10, analogous to IIB domains for other sugars (Pas & Robillard, 1988; Pas et al., 1988, 1991; Meins et al., 1993), because no other histidine or cysteine residue is conserved between the *E. coli* and *Bacillus stearothermophilus* IIB$^{cel}$ proteins (Lai & Ingram, 1993). The only other proteins, apart from enzymes IIB, that are known to involve phospho-cysteines are several protein tyrosine phosphate phosphatases (Guan & Dixon, 1991; Cho et al., 1992). No 3-dimensional structure is known of such an enzyme, either in the phosphorylated or in the unphosphorylated state. IIB$^{cel}$ is homologous to the B-domain of enzyme II$^{lac}$ of *Staphylococcus aureus*, with 25% identical residues (Reizer et al., 1990), and the region around the active site cysteine shows a similarity to the same re-

Reprint requests to: Ruud M. Scheek, The Groningen Biomolecular Science and Biotechnology Institute, University of Groningen, Nijenborgh 4, 9747 AG Groningen, The Netherlands; e-mail: scheek@chem.rug.nl.

*Abbreviations:* $^{15}N$-NOESY-HSQC, 3D $^{1}H$ NOE $^{1}H$-$^{15}N$ heteronuclear single-quantum coherence spectroscopy; $^{15}N$-TOCSY-HSQC, 3D $^{1}H$ total correlation $^{1}H$-$^{15}N$ heteronuclear single-quantum coherence spectroscopy; HNCA, HN(CO)CA, 3D $^{1}H$-$^{15}N$-$^{13}C\alpha$ correlation spectroscopy; HNCO, HN(CA)CO, 3D $^{1}H$-$^{15}N$-$^{13}CO$ correlation spectroscopy; COCAH, 3D $^{13}CO$-$^{13}C\alpha$-$^{1}H\alpha$ correlation spectroscopy; TPPI, time proportional phase incrementation; rf, radio frequency; PEP, phosphoenol-pyruvate; PMSF, phenylmethylsulfonyl fluoride; PTS, phosphoenol-pyruvate-dependent phosphotransferase system; mtl, mannitol; cel, cellobiose; HPr, histidine containing protein; EI, enzyme I; EII, enzyme II; TSP, trimethylsilylpropionic acid; TMS, trimethylsilylpropanesulfonic acid; TG, Tris-acetate/glycerol; IIA$^{cel}$, IIB$^{cel}$, IIC$^{cel}$, enzymes IIA, IIB, IIC of the cellobiose PTS; IIB$^{mtl}$, the B-domain of enzyme II mannitol.

gion in the B-domain of enzyme II$^{mtl}$ of *E. coli*. IIB$^{cel}$ shows no homology to the protein tyrosine phosphate phosphatases.

Previous attempts by us to perform NMR experiments on a subcloned IIB domain of the mannitol PTS (Robillard et al., 1993) were hampered by the apparent instability of this domain on a time scale of a few weeks, necessary to collect a complete set of NMR data. This instability could have been caused by oxidation of the active site cysteine and aggregation due either to oxidation or to the presence of flexible linker peptides at the N-terminus and the C-terminus of the recombinant protein, which remained after subcloning. Because IIB$^{cel}$ is a protein that occurs naturally as a separate, water-soluble domain, it was expected that we would have fewer instability problems than with IIB$^{mtl}$. To prevent complications arising from the oxidation of cysteine, we used a Cys 10 Ser mutant for our NMR experiments. Spin systems and through space connectivities were identified via 3D TOCSY-HSQC and 3D NOESY-HSQC experiments on $^{15}$N-labeled protein and HNCA, HN(CO)CA, HNCO, HN(CA)CO, and COCAH experiments on $^{13}$C/$^{15}$N-labeled protein.

## Results

The mutagenesis was confirmed by electrospray mass spectrometry and by N-terminal sequencing, both performed on purified, unlabeled protein. The measured molecular weight of the Cys 10 Ser mutant was 11,409.1 ± 1.0, which is in excellent agreement with the expected MW (11,409.4). N-terminal sequencing of the first 10 residues was in agreement with the sequence predicted from the DNA, including a serine at position 10.

Figures 1 and 2A show the $^{15}$N HSQC spectrum recorded with the $^{13}$C/$^{15}$N sample at 20 °C. The resolution in the $^{15}$N domain was fully exploited by taking 512 $t_2$ increments, and as a result, most resonances were well resolved. A few resonances show overlap, e.g., Ile 35 with Met 14, and Glu 46 with Lys 74. Resonances for all residues are present in Figure 1, except for Met 1 and Glu 2, whose amide protons probably exchange too rapidly with water to be observable. The $NH_2$ groups of Asn and Gln residues give rise to the expected number of additional pairs of peaks; they will be treated later. The high resolution seen in the $^{15}$N domain in Figures 1 and 2A cannot be attained in 3D spectra because of time limitations. Figure 2B compares a lower resolution $^1$H-$^{15}$N projection of the HNCO spectrum with the same region of the higher resolution $^{15}$N-HSQC spectrum in Figure 2A. The lower resolution in the $^{15}$N domain of the HNCA, HN(CO)CA, HNCO, and HN(CA)CO experiments did not cause ambiguities in the interpretation of these spectra because the traces in the $^{13}$C domain contain only 1 or 2 peaks for every $^1$H-$^{15}$N trace (see Fig. 3). However, for the $^{15}$N-TOCSY-HSQC and the $^{15}$N-NOESY-HSQC, it caused ambiguities in the assignment of H$\alpha$ resonances, which in the case of the TOCSY could be resolved by using the COCAH.

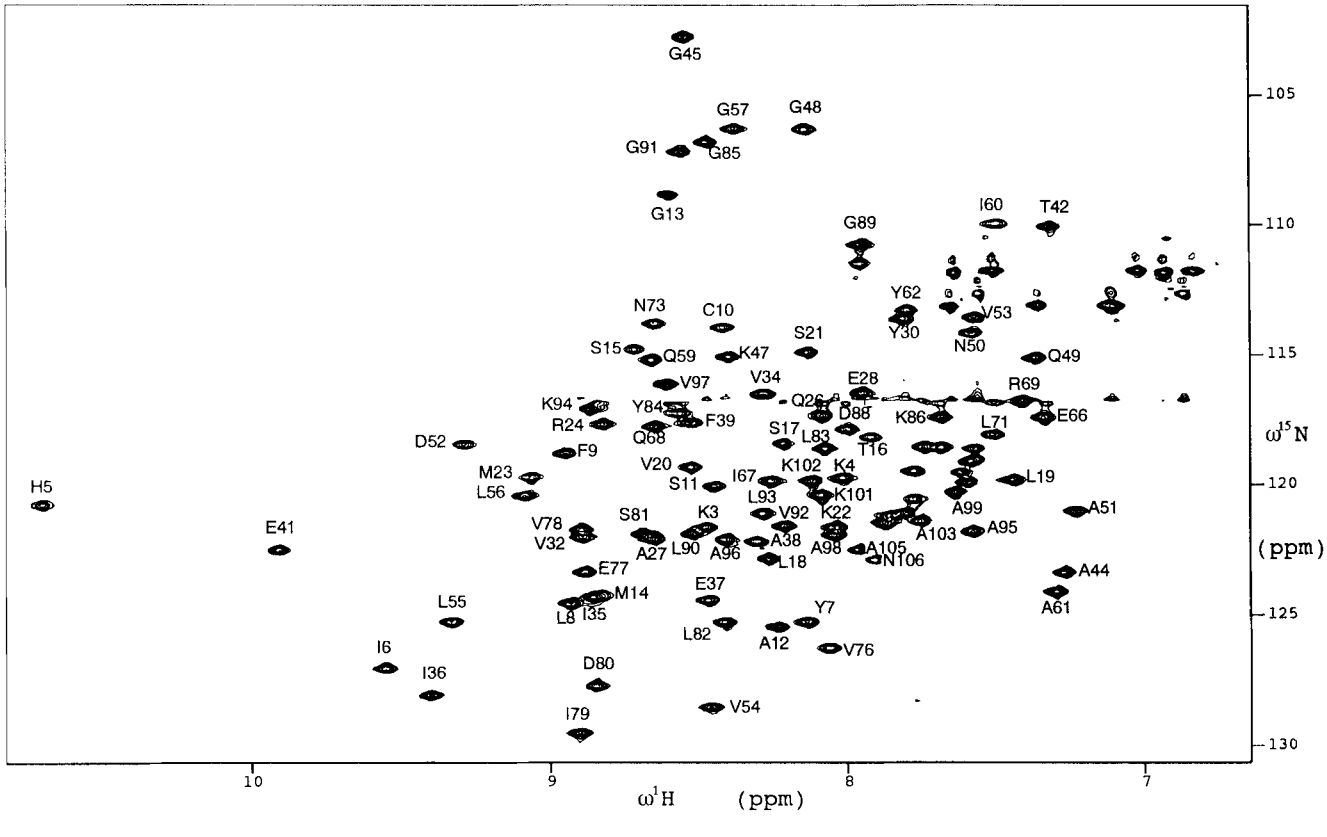


**Fig. 1.** High-resolution HSQC of IIB$^{cel}$. Conditions: 20 °C, TG-buffer, pH 6.2, 7% $D_2O$, 2 mM $^{13}$C/$^{15}$N IIB$^{cel}$. The spectral widths were 6,666.7 Hz ($^1$H) and 2,000 Hz ($^{15}$N). The maximum value for $t_1$ ($^{15}$N) was 128 ms, corresponding to 512 increments, and for $t_2$ ($^1$H) was 154 ms.

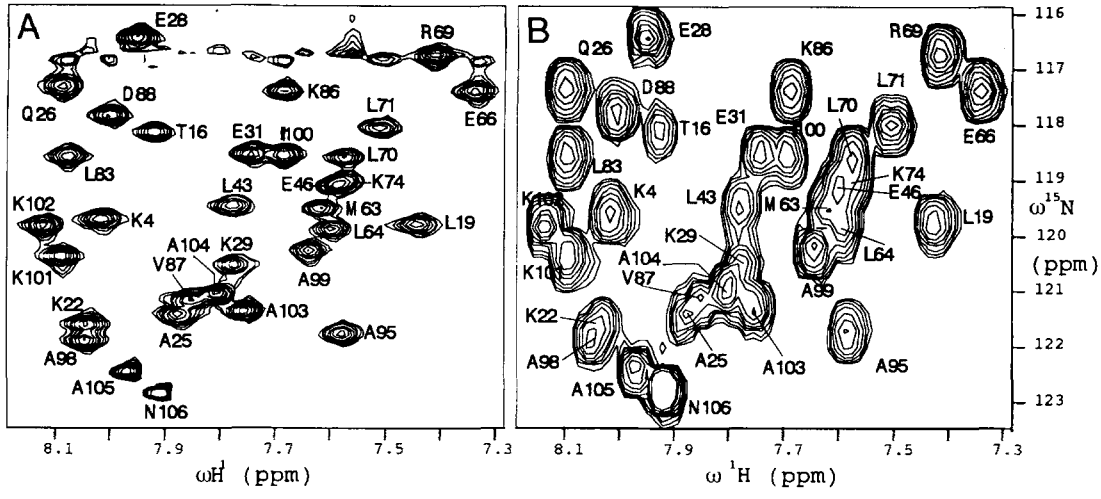


**Fig. 2.** Comparison of **(A)** $^{15}$N-HSQC with 512 increments in $t_1$ ($^{15}$N) and **(B)** HNCO projection in the $^1$H-$^{15}$N plane, with 128 $t_2$ increments in the $^{15}$N domain. The digital resolution of the $^{15}$N-HSQC spectrum in the $^{15}$N domain is 0.25 lines/Hz; in the HNCO spectrum it is 0.064 lines/Hz.

*Backbone assignments*

The HNCA, HN(CO)CA, HNCO, and HN(CA)CO spectra were used as the main source of information for sequential assignment. Each amide peak $^1$H-$^{15}$N($i$) in the $^1$H-$^{15}$N planes of the HNCA spectrum is labeled with the $^{13}$C$\alpha$ frequencies of the same residue, $^{13}$C$\alpha(i)$, and of the preceding residue, $^{13}$C$\alpha(i-1)$. The same peak in the HN(CO)CA spectrum is labeled only with the $^{13}$C$\alpha$ frequency of the preceding residue, $^{13}$C$\alpha(i-1)$. Using both the HNCA and HN(CO)CA spectra for every $^1$H-$^{15}$N

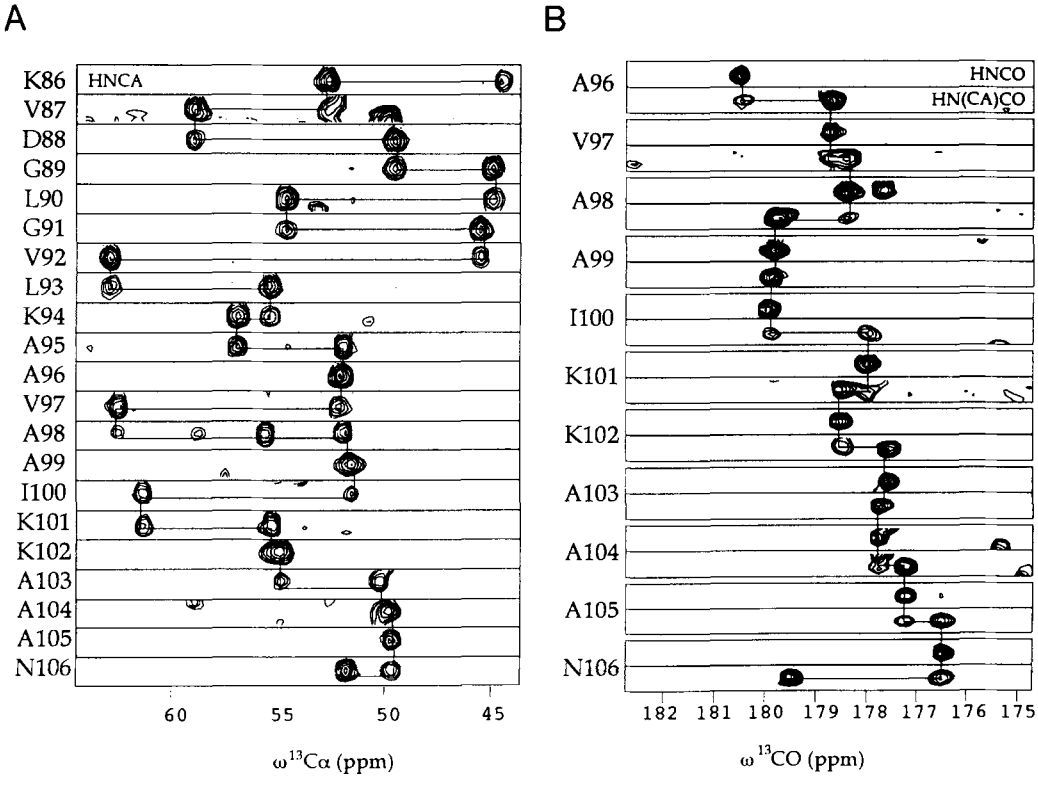


**Fig. 3. A:** Slices of the HNCA for the 21 C-terminal residues of IIB$^{cel}$, taken at their corresponding $^1$H-$^{15}$N frequencies. **B:** Alternating slices of the HN(CA)CO and HNCO for the 11 C-terminal residues of IIB$^{cel}$. For each residue 2 slices are shown, taken at the same $^1$H-$^{15}$N frequencies; the upper slice is from the HNCO for each residue, and the lower slice is from the HN(CA)CO.

pair enabled us to assign the $^{13}C\alpha$ frequency of the corresponding residue and the $^{13}C\alpha$ frequency of the preceding residue. Figure 3A shows the sequential correlation in the HNCA for the 21 C-terminal residues.

Each amide peak $^{1}H$-$^{15}N(i)$ in the $^{1}H$-$^{15}N$ planes of the HNCO spectrum is labeled with the $^{13}CO$ frequency of the preceding residue, $^{13}CO(i-1)$, but the same peak in the HN(CA)CO spectrum is labeled with the $^{13}CO$ frequencies of its own residue, $^{13}CO(i)$, and, notably, the preceding residue, $^{13}CO(i-1)$. To our knowledge, the correlation with the $^{13}CO$ frequency of the preceding residue in a HN(CA)CO experiment is not usually observed; however, we observed this correlation in about 90% of the traces, so we used this information systematically, as in the HNCA. The presence of both correlations is shown in Figure 3B, where a sequential arrangement of HNCO and HN(CA)CO slices of the 11 C-terminal residues is presented. One would expect this kind of correlation, just as in the HNCA, because in the coherence transfer time of 25 ms not only the 1-bond $^{1}J_{N(i)C\alpha(i)}$ coupling (8–12 Hz) but also the 2-bond $^{2}J_{N(i)C\alpha(i-1)}$ coupling (~6 Hz) will develop. Using the HNCO and HN(CA)CO spectra for every $^{1}H$-$^{15}N$ pair enabled us to assign the $^{13}CO$ frequency of the corresponding residue, $^{13}CO(i)$, and the preceding residue, $^{13}CO(i-1)$.

The HNCA, HN(CO)CA, HNCO, and HN(CA)CO peak lists were used to identify possible sequential relationships. Ambiguities in the assignment of neighbors because of overlap in both $^{13}C\alpha$ and $^{13}CO$ frequencies could be resolved by using the $^{15}N$-TOCSY-HSQC and $^{15}N$-NOESY-HSQC spectra. Assignment of the resonances to specific residues in the amino acid sequence of IIB$^{cel}$ was started from short stretches with spin systems that could easily be identified, such as glycine by its TOCSY trace and by its characteristic C$\alpha$ shift, and alanine by its TOCSY trace. Some of these stretches could relatively easily be positioned in the sequence, and served as starting points for further assignments. The chemical shifts of the backbone $^{1}HN$, $^{15}N$, $^{13}C\alpha$, and $^{13}CO$ atoms of all non-proline residues in the sequence were completely assigned in this manner, apart from the first 2 residues, which show no peaks in $^{15}N$-$^{1}H$-HSQC spectra. The $^{13}C\alpha$ and $^{13}CO$ chemical shifts of Glu 2 were assigned using the HNCA and HN(CA)CO traces of Lys 3. The $^{1}H\alpha$ chemical shift of Glu 2 was identified from the $^{13}C\alpha$ and $^{13}CO$ frequencies of Glu 2 in the COCAH spectrum. The COCAH spectrum together with sequential information from the HNCA and HN(CA)CO spectra also yielded the $^{13}C\alpha$, $^{13}CO$, and $^{1}H\alpha$ chemical shifts of all proline residues. This left 1 strong peak unassigned in the $^{13}C\alpha$-$^{13}CO$-$^{1}H\alpha$ region of the COCAH spectrum. This peak was tentatively assigned to Met 1. All the backbone assignments are listed in Table 1.

### *Secondary structure*

The deviation of $^{1}H\alpha$ and $^{13}C\alpha$ chemical shifts from their random coil values as measured in small peptides, the "secondary shift," is indicative of the type of secondary structure that is present (Spera & Bax, 1991; Wishart et al., 1992). Figure 4A shows the $^{1}H\alpha$, $^{13}C\alpha$, and $^{13}CO$ secondary shift for each residue of IIB$^{cel}$. The $^{13}CO$ secondary shift shows the same tendency as the $^{13}C\alpha$ secondary shift: positive values in helices and negative values in $\beta$-sheets, although the effect is somewhat less pronounced. The short-range NOE information, shown in Figure 4B, also gives information about the secondary structure (Wüthrich, 1986). The presence of $\alpha N(i, i+3)$ NOEs and strong $NN(i, i+1)$ NOEs is characteristic of helices, whereas strong $\alpha N(i, i+1)$ NOEs are characteristic of $\beta$-strands. In Figure 4B, the NOE crosspeaks were classified as weak, medium, and strong. A region was considered helical if a combination of $NN(i, i+1)$ NOEs and $\alpha N(i, i+3)$ NOEs with weak $\alpha N(i, i+1)$ NOEs was present, together with positive $^{13}C\alpha$ and negative $^{1}H\alpha$ secondary shifts. The $\beta$-strands were roughly located on the basis of the presence of strong or medium $\alpha N(i, i+1)$ NOEs, the absence of unambiguously assigned $\alpha N(i, i+3)$ NOEs, positive $^{1}H\alpha$ secondary shift, and negative $^{13}C\alpha$ secondary shift. A more accurate determination of the $\beta$-strand regions is derived from inter-$\beta$-strand $N\alpha(i, j)$ NOEs. An analysis of these NOEs revealed that IIB$^{cel}$ possesses a 4-stranded parallel $\beta$-sheet, as shown in Figure 5.

## Discussion

The NMR resonances of almost all backbone atoms of the Cys 10 Ser mutant of IIB$^{cel}$ have been assigned. An analysis of $^{1}H\alpha$, $^{13}C\alpha$, $^{13}CO$ chemical shifts and short- and long-range NOE crosspeaks revealed that IIB$^{cel}$ consists of 5 helices and a 4-stranded parallel $\beta$-sheet. In the wild-type enzyme, the catalytic residue Cys 10 would be located in the $\beta$-sheet close to the N-terminal side of the first helix. In the phosphorylated state of the enzyme, the negatively charged phosphoryl group could interact favorably with the helix dipole. IIB$^{cel}$ is homologous to the B-domain of enzyme II$^{lac}$, so these proteins probably have similar structures. There is no obvious homology of IIB$^{cel}$ with IIB$^{mtl}$, except at the active site. A short stretch of the sequence of IIB$^{cel}$ around the phosphorylation site, Cys 10 (IYLFCSAGMSTS), shows similarity to the sequence of IIB$^{mtl}$ around Cys 384 (IIVACDAGMGSS) (Lee & Saier, 1983). This might indicate a similarity in structure of the active sites and possibly of these 2 proteins. Work is under way in our laboratory to complete the side-chain resonance assignments and determine the 3D structure of IIB$^{cel}$.

## Materials and methods

### *Expression vectors and bacterial strains*

The overexpression plasmid pJR-IIBC10S was constructed as follows. First, the 849-bp *Hin* dIII fragment from pUF673 (Parker & Hall, 1990) was cloned into the *Hin* dIII site of pBluescript SK (Stratagene, La Jolla, California). The IIB$^{cel}$-encoding DNA in the resulting vector (pJR-BLIIB) was then used to create, by site-directed mutagenesis, an *Nde* 1 site in the initiation codon of celA and to change the cysteine residue at position 10 to serine. In the last step, the *Nde* 1–*Sal* 1 fragment containing the mutant C10S of the IIB$^{cel}$-encoding gene was placed between the *Nde* 1 and *Sal* 1 of pJL503. Site-directed mutagenesis was performed as described by Nakamaye and Eckstein (1986). The oligodeoxynucleotides used to create the *Nde* 1 site and the C10S substitution were 5′-TTT CTT TTC CAT ATG ACT GCC CTC-3′ and 5′-GCC CGC AGA ACT AAA CAG ATA AAT-3′, respectively. The plasmid pJR-IIBC10S, containing the *cel*A gene with the C10S mutation, was transformed to *E. coli* strains TOPP4 *rif*$^{r}$ (F′, *proAB*, *lacI*$^{q}$*ZΔM15*, Tn*10*, (*tet*$^{r}$)) (Stratagene) for $^{15}N$ labeling and *E. coli* W3110 for

**Table 1.** *Backbone $^{1}H$, $^{15}N$, and $^{13}C$ chemical shifts of $IIB^{cel}$ of E. coli in TG-buffer pH 6.2, 20 °C*[a]

| Residue | $^{1}HN$ | $^{15}N$ | $^{1}H\alpha$ | $^{13}C\alpha$ | $^{13}CO$ | Residue | $^{1}HN$ | $^{15}N$ | $^{1}H\alpha$ | $^{13}C\alpha$ | $^{13}CO$ |
|---|---|---|---|---|---|---|---|---|---|---|---|
| 1 Met[b] | | | 4.12 | 54.8 | 172.1 | 55 Leu | 9.30 | 125.3 | 5.60 | 51.9 | 175.8 |
| 2 Glu | | | 4.37 | 56.1 | 175.7 | 56 Leu | 9.06 | 120.5 | 5.16 | 52.4 | 176.6 |
| 3 Lys | 8.45 | 121.7 | 4.36 | 56.1 | 176.5 | 57 Gly | 8.36 | 106.3 | 3.84 | 44.0 | 171.0 |
| 4 Lys | 7.99 | 119.8 | 4.57 | 54.0 | 175.8 | | | | 3.81 | | |
| 5 His | 10.67 | 120.8 | 5.05 | 55.6 | 174.6 | 58 Pro | | | 4.00 | 65.0 | 179.1 |
| 6 Ile | 9.53 | 127.1 | 4.43 | 60.2 | 173.5 | 59 Gln | 8.64 | 115.2 | 4.24 | 58.0 | 177.4 |
| 7 Tyr | 8.11 | 125.3 | 6.00 | 52.1 | 173.2 | 60 Ile | 7.47 | 109.9 | 4.64 | 59.9 | 175.7 |
| 8 Leu | 8.91 | 124.6 | 5.41 | 54.1 | 175.1 | 61 Ala | 7.27 | 124.1 | 3.76 | 55.6 | 179.7 |
| 9 Phe | 8.92 | 118.8 | 5.69 | 56.0 | 174.6 | 62 Tyr | 7.77 | 113.3 | 4.36 | 58.4 | 176.1 |
| 10 Ser | 8.40 | 113.9 | 4.62 | 57.1 | 172.7 | 63 Met | 7.59 | 119.5 | 4.20 | 56.1 | 175.7 |
| 11 Ser | 8.42 | 120.1 | 4.92 | 57.7 | 174.4 | 64 Leu | 7.57 | 119.9 | 3.85 | 60.9 | 173.3 |
| 12 Ala | 8.21 | 125.5 | 4.44 | 52.3 | 177.7 | 65 Pro | | | 4.43 | 65.9 | 179.6 |
| 13 Gly | 8.58 | 108.8 | 4.12 | 46.2 | 175.5 | 66 Glu | 7.31 | 117.4 | 4.16 | 58.5 | 178.5 |
| | | | 3.72 | | | 67 Ile | 8.23 | 119.9 | 3.60 | 63.8 | 177.6 |
| 14 Met | 8.80 | 124.2 | 4.36 | 58.1 | 177.7 | 68 Gln | 8.63 | 117.8 | 4.00 | 58.6 | 178.5 |
| 15 Ser | 8.69 | 114.8 | 4.17 | 61.2 | 176.7 | 69 Arg | 7.38 | 116.8 | 3.97 | 58.5 | 178.3 |
| 16 Thr | 7.89 | 118.2 | 4.03 | 65.5 | 174.9 | 70 Leu | 7.55 | 118.6 | 4.08 | 56.6 | 176.8 |
| 17 Ser | 8.19 | 118.4 | 3.99 | 62.1 | 176.9 | 71 Leu | 7.48 | 118.1 | 4.77 | 51.0 | 173.3 |
| 18 Leu | 8.24 | 122.9 | 4.15 | 57.7 | 179.0 | 72 Pro | | | 4.46 | 64.5 | 177.6 |
| 19 Leu | 7.42 | 119.8 | 3.84 | 58.1 | 178.5 | 73 Asn | 8.63 | 113.8 | 4.68 | 53.0 | 174.4 |
| 20 Val | 8.50 | 119.3 | 3.48 | 67.2 | 177.9 | 74 Lys | 7.55 | 119.1 | 4.86 | 52.0 | 173.8 |
| 21 Ser | 8.11 | 114.9 | 4.14 | 62.2 | 177.6 | 75 Pro | | | 4.66 | 62.8 | 175.1 |
| 22 Lys | 8.01 | 121.7 | 4.29 | 58.9 | 179.6 | 76 Val | 8.03 | 126.3 | 5.09 | 60.4 | 175.0 |
| 23 Met | 9.04 | 119.7 | 3.65 | 60.3 | 178.0 | 77 Glu | 8.86 | 123.4 | 4.71 | 53.8 | 174.7 |
| 24 Arg | 8.80 | 117.7 | 3.88 | 60.0 | 178.9 | 78 Val | 8.87 | 121.8 | 4.29 | 61.4 | 176.7 |
| 25 Ala | 7.85 | 121.5 | 4.25 | 55.0 | 181.4 | 79 Ile | 8.87 | 129.6 | 3.73 | 62.6 | 174.4 |
| 26 Gln | 8.06 | 117.4 | 4.28 | 57.7 | 177.4 | 80 Asp | 8.81 | 127.7 | 4.35 | 55.6 | 177.4 |
| 27 Ala | 8.63 | 122.1 | 3.95 | 55.2 | 179.6 | 81 Ser | 8.66 | 121.9 | 3.92 | 62.3 | 176.8 |
| 28 Glu | 7.93 | 116.5 | 4.11 | 58.8 | 179.4 | 82 Leu | 8.39 | 125.3 | 4.32 | 57.8 | 179.8 |
| 29 Lys | 7.75 | 120.6 | 3.91 | 58.9 | 177.5 | 83 Leu | 8.05 | 118.6 | 3.99 | 58.0 | 179.4 |
| 30 Tyr | 7.79 | 113.6 | 4.54 | 58.4 | 173.6 | 84 Tyr | 8.54 | 117.3 | 3.78 | 62.4 | 179.3 |
| 31 Glu | 7.72 | 118.6 | 3.89 | 57.0 | 175.4 | 85 Gly | 8.45 | 106.8 | 4.10 | 46.8 | 175.4 |
| 32 Val | 8.86 | 122.0 | 4.36 | 59.8 | 176.4 | | | | 3.94 | | |
| 33 Pro | | | 4.75 | 62.3 | 174.4 | 86 Lys | 7.66 | 117.4 | 4.30 | 55.7 | 175.4 |
| 34 Val | 8.26 | 116.5 | 5.41 | 58.3 | 174.3 | 87 Val | 7.82 | 121.2 | 2.98 | 62.4 | 174.9 |
| 35 Ile | 8.83 | 124.3 | 4.30 | 59.8 | 174.1 | 88 Asp | 7.97 | 117.9 | 4.65 | 52.2 | 175.5 |
| 36 Ile | 9.37 | 128.1 | 5.42 | 59.6 | 175.0 | 89 Gly | 7.93 | 110.8 | 3.58 | 47.1 | 174.7 |
| 37 Glu | 8.44 | 124.5 | 4.41 | 54.6 | 172.7 | | | | 3.33 | | |
| 38 Ala | 8.28 | 122.2 | 5.33 | 49.3 | 175.6 | 90 Leu | 8.50 | 121.9 | 4.06 | 57.8 | 177.8 |
| 39 Phe | 8.50 | 117.6 | 4.94 | 55.3 | 172.9 | 91 Gly | 8.54 | 107.2 | 3.70 | 47.7 | 177.2 |
| 40 Pro | | | 4.93 | 62.5 | 178.2 | | | | 3.60 | | |
| 41 Glu | 9.88 | 122.5 | 4.13 | 59.5 | 176.5 | 92 Val | 8.19 | 121.6 | 3.71 | 66.7 | 177.6 |
| 42 Thr | 7.29 | 110.1 | 4.14 | 62.8 | 175.8 | 93 Leu | 8.26 | 121.1 | 3.88 | 58.6 | 177.8 |
| 43 Leu | 7.75 | 119.5 | 4.68 | 54.0 | 177.1 | 94 Lys | 8.84 | 117.1 | 3.79 | 60.3 | 179.7 |
| 44 Ala | 7.25 | 123.4 | 2.69 | 55.8 | 178.5 | 95 Ala | 7.55 | 121.8 | 4.18 | 54.9 | 180.5 |
| 45 Gly | 8.52 | 102.7 | 3.75 | 46.6 | 174.2 | 96 Ala | 8.38 | 122.1 | 3.97 | 55.0 | 178.6 |
| | | | 3.49 | | | 97 Val | 8.58 | 116.1 | 3.50 | 66.4 | 178.3 |
| 46 Glu | 7.57 | 119.2 | 4.25 | 57.9 | 178.2 | 98 Ala | 8.02 | 122.0 | 4.11 | 54.7 | 179.8 |
| 47 Lys | 8.38 | 115.1 | 4.29 | 55.4 | 178.9 | 99 Ala | 7.61 | 120.3 | 4.18 | 54.3 | 179.9 |
| 48 Gly | 8.12 | 106.3 | 4.07 | 47.0 | 174.1 | 100 Ile | 7.66 | 118.6 | 3.55 | 65.1 | 178.0 |
| | | | 3.62 | | | 101 Lys | 8.06 | 120.4 | 4.07 | 58.5 | 178.5 |
| 49 Gln | 7.34 | 115.1 | 3.98 | 58.0 | 176.6 | 102 Lys | 8.09 | 119.9 | 4.11 | 58.1 | 177.5 |
| 50 Asn | 7.56 | 114.2 | 4.85 | 52.1 | 173.8 | 103 Ala | 7.73 | 121.4 | 4.26 | 53.0 | 177.7 |
| 51 Ala | 7.20 | 121.0 | 3.54 | 51.4 | 176.0 | 104 Ala | 7.78 | 121.1 | 4.30 | 52.4 | 177.2 |
| 52 Asp | 9.26 | 118.5 | 4.88 | 56.3 | 175.4 | 105 Ala | 7.94 | 122.5 | 4.33 | 52.3 | 176.5 |
| 53 Val | 7.55 | 113.5 | 4.41 | 61.0 | 171.0 | 106 Asn | 7.88 | 122.9 | 4.46 | 54.6 | 179.6 |
| 54 Val | 8.43 | 128.6 | 4.80 | 61.2 | 173.3 | | | | | | |

[a] The $^{1}H$ chemical shifts are relative to TSP, the $^{15}N$ chemical shifts are relative to liquid $NH_3$ (Live et al., 1984), and the $^{13}C\alpha$ and $^{13}CO$ chemical shifts are relative to hypothetical internal TSP (Bax & Subramanian, 1986).

[b] Tentative assignments from COCAH.

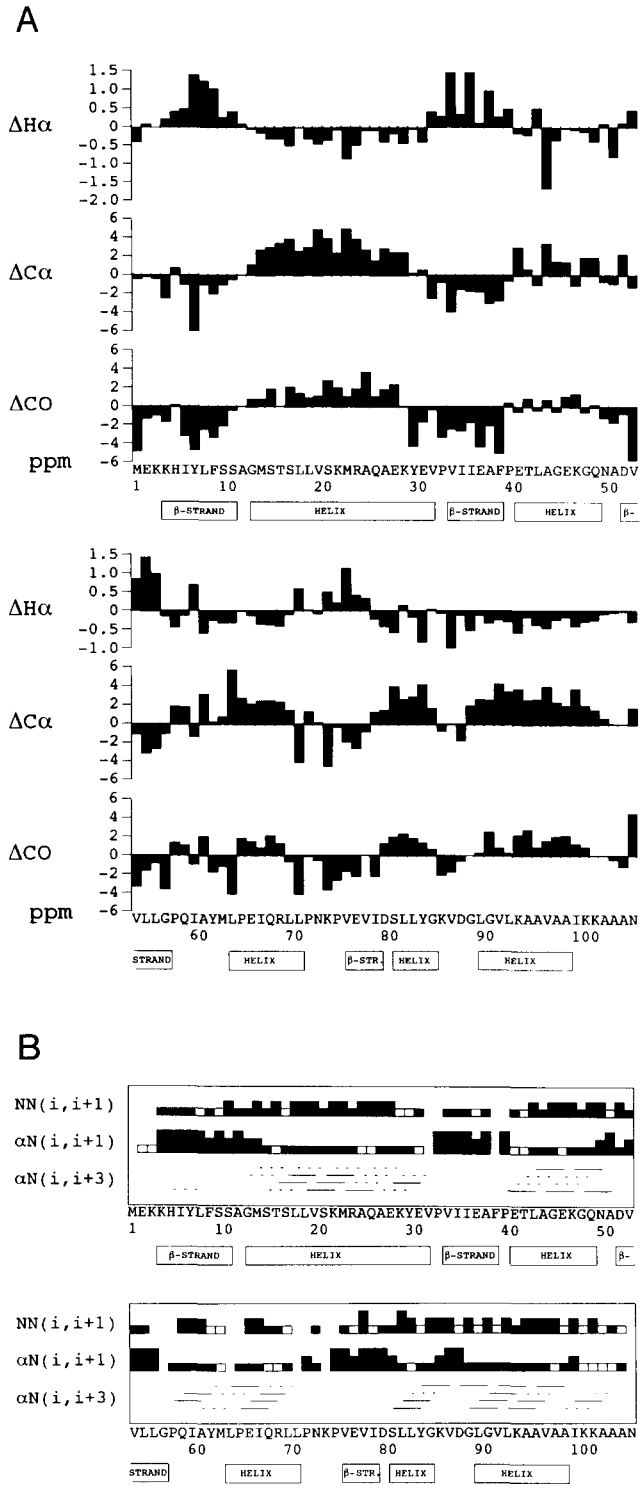


**Fig. 4.** Secondary structure indicators. **A:** Secondary shift for backbone $^1H\alpha$ ($\Delta H\alpha$), $^{13}C\alpha$ ($\Delta C\alpha$), and $^{13}CO$ ($\Delta CO$) resonances. The $^{13}CO$ secondary shifts are calculated using random coil values relative to TMS (Howarth & Lilley, 1978). The $^1H\alpha$ secondary chemical shifts of the glycines are calculated by subtracting the average chemical shift of the 2 H$\alpha$'s from the random coil value (Wishart et al., 1992). **B:** Short-range NOE contacts. The $\alpha N(i, i+1)$ and $NN(i, i+1)$ connectivities correspond to strong, medium, and weak NOEs, represented by large, medium, and small bars, respectively. The open bars in the $\alpha N(i, i+1)$ and $NN(i, i+1)$ connectivities and the dashed lines in the $\alpha N(i, i+3)$ connectivities represent ambiguities due to spectral overlap.

$^{13}C/^{15}N$ labeling using standard procedures (Sambrook et al., 1989).

### *Production of uniformly $^{15}N$-enriched IIB$^{cel}$*

The cells were grown in M9 mineral medium (Sambrook et al., 1989) containing 2 mg/L thiamine, 0.09 mM $CaCl_2$, 0.9 mM $MgSO_4$, 1 g/L $^{15}N_2$-ammonium sulfate (99.9% enriched; Isotec, Inc., Miamisburg, Ohio), and 4 g/L glucose. A 20-mL overnight culture of unlabeled M9 medium containing 12.5 μg/mL tetracycline and 100 μg/mL ampicillin was used to inoculate 2 L of labeled M9 medium without ampicillin. The temperature was shifted to 42 °C after growing at 30 °C until $OD_{600} = 0.6$. Cells were harvested by centrifugation after 135 min at 42 °C.

### *Production of uniformly $^{13}C/^{15}N$-enriched IIB$^{cel}$*

Doubly labeled IIB$^{cel}$ was produced in the same way as above with the following modifications. *E. coli* strain W3110 was used instead of TOPP4 because it showed a higher expression of IIB$^{cel}$ at low glucose concentrations. W3110 was grown in 3 L of M9 medium containing 1 g/L $^{15}N_2$-ammonium sulfate (99.9% enriched; Isotec, Inc.), 1 g/L $^{13}C_6$-glucose (99% enriched; Cambridge Isotope Laboratories, Cambridge, Massachusetts). Tetracycline was omitted from all media. Trace metals were added at a ratio of 1 mL stock solution per liter of medium, using the following stock solutions: (a) 1 g EDTA, 30 mg $ZnSO_4 \cdot 7H_2O$, 198 mg $MnCl_2 \cdot 4H_2O$, 254 mg $CoCl_2 \cdot 4H_2O$, 13.4 mg $CuCl_2$, and 147 mg $CaCl_2$ in 100 mL water; the solution was brought to pH 4 with NaOH; and (b) 278 mg $FeSO_4 \cdot 7H_2O$ in 1 N HCl. Cells were harvested by centrifugation after 4 h at 42 °C.

### *Purification and characterization*

Cells were resuspended in 100 mL of TG-buffer (10 mM Tris-acetate, pH 6.5, containing 5% glycerol, 1 mM $NaN_3$, 1 mM dithiothreitol) with 1 mM phenylmethylsulfonyl fluoride (PMSF) and stored at −20 °C. The cell suspension was passed through a French press at 5,000–10,000 psi. Membranes were sedimented by centrifugation (150,000 × *g*, 4 °C, 45 min), and the pellet was homogenized with 50 mL TG-buffer and centrifuged again. Both supernatants were combined and loaded on an S-Sepharose column (15 × 2.5 cm) at a flow rate of 1 mL/min, after which the column was washed overnight with TG-buffer. Elution was performed with a gradient of 2 × 250 mL of 0–300 mM NaCl in the same buffer. Fractions were pooled on the basis of the pattern seen on SDS-PAGE gels. Fractions containing IIB$^{cel}$ were loaded onto a G-50 Sephadex column (80 × 3.5 cm), after adjusting the NaCl concentration to 100 mM, and gel filtration was then carried out using TG-buffer at pH 6.5 with 100 mM NaCl. A total of 20 mg IIB$^{cel}$ was obtained for both the $^{15}N$ and the $^{13}C/^{15}N$ IIB$^{cel}$ samples. These were then concentrated to a volume of 0.6 mL using Centricon concentrators with a cut-off of 3 kDa. $D_2O$ was added to 7%, and EDTA was added to 2 mM. After purification, the final pH of the $^{13}C/^{15}N$ IIB$^{cel}$ sample was 6.2. The purity of the purified IIB$^{cel}$ was estimated to be >95% from 15% SDS-PAGE gels (Laemmli et al., 1970) stained with Coomassie brilliant blue.

The protein was characterized by determining its molecular weight using electron spray mass spectroscopy and N-terminal

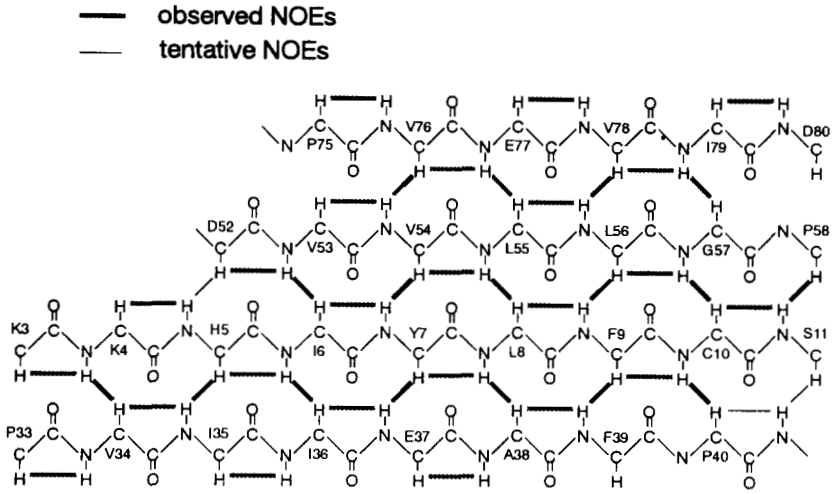


**Fig. 5.** The 4-stranded parallel $\beta$-sheet of IIB$^{cel}$ of *E. coli*. Thick lines correspond to unambiguously assigned NOEs; thin lines represent NOEs that were not unambiguously assigned, due to spectral overlap.

sequencing of the first 15 residues of the purified protein. Mass spectrometry was performed on a TSQ 700 instrument (Finnigan Mat, San Jose, California) fitted with an electrospray ion source. Samples were diluted in 1/1 (V/V) methanol/water containing 1% acetic acid to a final concentration of 10 pmol/L. Using a syringe pump (Havard Apparatus, South Natick, Massachusetts), the samples were introduced into the ion source through a fused silica capillary at a flow rate of 3 L/min. Tuning and calibration of the instrument were performed using horse myoglobin. Positive full-scan mass spectra were acquired over the *m/z* range 950–1,950. Approximately 40 scans were averaged and deconvoluted to give the corresponding mass of the protein using the Bio Mass Program (Finnigan Mat). Sequencing was done by Edman degradation on the purified protein using a Knauer model 810 pulsed liquid sequenator (Knauer, Berlin, Germany) according to the instructions of the manufacturer.

For experiments in $D_2O$, the $^{13}C/^{15}N$ sample was repeatedly diluted with TG-buffer in $D_2O$ containing $D_5$-glycerol and concentrated again. The protein concentration was determined using the Bradford (1976) method with bovine serum albumin as a standard. The concentration of the $^{15}N$ NMR sample was ~4 mM; that of the $^{13}C/^{15}N$ NMR sample was ~2 mM.

### *The $^{15}N$-$^{1}H$ HSQC experiment*

All NMR experiments were performed on a Varian Unity 500-MHz spectrometer. The $^{15}N$-HSQC spectrum (Bodenhausen & Ruben, 1980) was recorded at 20 °C (Fig. 1) using the $^{13}C/^{15}N$ sample. The spectral widths were 6,666.7 Hz ($^{1}H$) and 2,000.0 Hz ($^{15}N$). The maximum values for $t_1$ ($^{15}N$) and $t_2$ ($^{1}H$) were 128 ms and 154 ms. The $^{1}H$ carrier was placed at the water frequency (4.81 ppm relative to TSP). The $^{15}N$ carrier was placed at 116.84 ppm relative to liquid $NH_3$. During $^{15}N$ evolution, $^{13}C\alpha$ decoupling was done using a GARP sequence with an rf field of $\gamma B_1 = 2$ kHz (Shaka et al., 1985), and $^{13}CO$ decoupling was done using a block wave with a modulation frequency of 90 Hz and an rf field of $\gamma B_1 = 0.5$ kHz. During acquisition, a broadband WALTZ-16 sequence (Shaka et al., 1983) with an rf field of $\gamma B_1 = 0.8$ kHz was used for $^{15}N$ decoupling. Water was suppressed by 2 orthogonal spin lock pulses of 2 and 6 ms applied during the reversed INEPT part of the pulse sequence.

### *$^{1}H$-$^{15}N$ heteronuclear 3D NMR spectroscopy*

The 3D $^{15}N$-NOESY-HSQC and 3D $^{15}N$-TOCSY-HSQC spectra were recorded at 20 °C using published pulse sequences (Fesik & Zuiderweg, 1988, 1990; Marion et al., 1989a, 1989b; Zuiderweg & Fesik, 1989; Norwood et al., 1990). The spectral widths in the $\omega 1$ ($^{1}H$), $\omega 2$ ($^{15}N$), and $\omega 3$ ($^{1}H$) domains of the spectra were 7,000.4, 2,000, and 7,000.4 Hz, respectively. The maximum values of $t_1$, $t_2$, and $t_3$ were 22.25, 18.3, and 146 ms. In order to obtain quadrature detection in $\omega 1$ and $\omega 2$, time proportional phase incrementation was used (Bodenhausen et al., 1980; Marion & Wüthrich, 1983). The $^{1}H$ carrier frequency was placed at the water resonance and the $^{15}N$ carrier at 116.84 ppm relative to liquid $NH_3$. The mixing time in the NOESY-HSQC experiment was 100 ms, including a 30-ms homospoil pulse in the middle of this period to remove any coherences of order 1 and higher. An MLEV17 sequence (Bax & Davis, 1985) was applied during the 37.4-ms spin lock period in the TOCSY-HSQC experiment, with an rf field of $\gamma B_1 = 11.8$ kHz and with 42.4-$\mu$s delays bracketing the $\pi$ pulses in the MLEV17 sequence (Griesinger et al., 1988). Water was suppressed by 2 orthogonal spin lock pulses of 2 and 4 ms applied during the reversed INEPT part of the pulse sequence (Messerle et al., 1989). During acquisition, a broadband WALTZ-16 sequence (Shaka et al., 1983) with an rf field of $\gamma B_1 = 0.8$ kHz was used for $^{15}N$ decoupling. Each experiment was acquired in 6–7 days.

### *$^{1}H$-$^{15}N$-$^{13}C$ triple resonance NMR spectroscopy*

The HNCA (Kay et al., 1990), HN(CO)CA (Bax & Ikura, 1991), HNCO (Grzesiek & Bax, 1992), and HN(CA)CO (Clubb et al., 1992) spectra were recorded using a constant time $^{13}C$ evolution period. All spectra were recorded at 20 °C. The $^{1}H$ carrier was placed at the water resonance (4.81 ppm relative to TSP), and the $^{15}N$ carrier was placed at 116.84 ppm relative to liquid $NH_3$. The $^{13}C\alpha$ and $^{13}CO$ carriers were placed at 58.18 and 177.51 ppm, respectively, relative to TSP. The spectral widths in the $^{1}H$, $^{15}N$, $^{13}C\alpha$, and $^{13}CO$ domains were 7,000.4, 2,000.0, 5,000.0, and 2,500.0 Hz, respectively. The maximum values for $t_1$ ($^{15}N$) and $t_3$ ($^{1}H$) were 15.25 ms and 73 ms for all experiments. The maximum values for $t_2$ ($^{13}C$) were 7.4 ms for the HNCA, 8.9 ms for the HN(CO)CA, 19.8 ms for the HNCO, and

13.8 ms for the HN(CA)CO. Quadrature detection in ω1 and ω2 was done using TPPI. The water signal was suppressed by a weak rf field during the preparation period of 1 s. The total experiment times were 6.8 days for the HNCA, 2.9 days for the HN(CO)CA, 1.7 days for the HNCO, and 5 days for the HN(CA)CO.

The COCAH experiment (Kroon et al., 1993; Dijkstra et al., 1994) had 2 constant time $^{13}C$ evolution periods and was recorded in TG-buffer with $D_2O$ and $D_5$-glycerol. The spectral widths in the $^{13}C\alpha$ (ω1), $^{13}CO$ (ω2), and $^{1}H\alpha$ (ω3) domains were 5,000, 2,500, and 7,000.4 Hz, respectively. The $^{1}H$ carrier was placed at the water resonance (4.81 ppm relative to TSP), and the $^{13}C\alpha$ and $^{13}CO$ carriers were placed at 56.18 ppm and 175.52 ppm, respectively, relative to TSP. The maximum values for $t_1$, $t_2$, and $t_3$ were 6.4, 18, and 73 ms, respectively. During both evolution periods, $^{15}N$ decoupling was done using a WALTZ-16 sequence. Water was suppressed by presaturating for 1 s during the 2-s relaxation delay. The total duration of the experiment was 5 days.

### *Data processing and analysis*

All data were processed on either a Convex C220 or a Silicon Graphics IRIS Indigo, using the program SNARF, written by Frans van Hoesel, Groningen. The 3D spectra were recorded as sets of 2D spectra. Before Fourier transformation, the $t_1$ and $t_2$ time domain data were extended by linear prediction and filtered by multiplication with a suitable window function (sine-bell or Lorentz–Gauss transformation). After Fourier transformation in all 3 domains, a data set of 1,024 (ω3, $^{1}H$) × 128 (ω2, $^{15}N$) × 512 (ω1, $^{1}H$) points was obtained in the case of the NOESY-HSQC and TOCSY-HSQC spectra. A data set of 1,024 (ω3, $^{1}H$) × 128 (ω2, $^{15}N$) × 128 (ω1, $^{13}C$) real points was obtained for the HNCA, HN(CO)CA, HNCO, and HN(CA)CO experiments, and a data set of 1,024 (ω3, $^{1}H$) × 128 (ω2, $^{13}C$) × 128 (ω1, $^{13}C$) real points was obtained for the COCAH experiment. A data set of 1,024 (ω3, $^{1}H$) × 512 (ω2, $^{15}N$) real points was obtained for the high-resolution 2D $^{15}N$-HSQC.

### *Determination of secondary structure*

Information concerning the secondary structure was obtained both from the deviations of the chemical shifts of Hα, Cα, and carbonyl resonances from their random coil values in small peptides and from the occurrence and magnitude of HN–HN and HN–Hα NOESY crosspeaks.

## Acknowledgments

We thank Varian for providing us with the triple-resonance probe; T. Nowak for assistance in acquiring the [$^{13}C$]glucose; Frans van Hoesel for writing the program SNARF, which we used for processing, visualization, and analyzing all NMR data sets; and J. van der Oost for supplying us with the TOPP4 strain.

## References

Bax A, Davis DG. 1985. MLEV-17 based two-dimensional homonuclear magnetization transfer spectroscopy. *J Magn Reson 65*:355–360.

Bax A, Ikura M. 1991. An efficient 3D NMR technique for correlating the proton and $^{15}N$ backbone amide resonances with the α-carbon of the preceding residue in uniformly $^{15}N/^{13}C$ enriched proteins. *J Biomol NMR 1*:99–104.

Bax A, Subramanian S. 1986. Sensitivity-enhanced two-dimensional heteronuclear shift correlation NMR spectroscopy. *J Magn Reson 67*:565–569.

Bodenhausen G, Ruben DJ. 1980. Natural abundance nitrogen 15 NMR by enhanced heteronuclear spectroscopy. *Chem Phys Lett 69*:185–189.

Bodenhausen G, Vold RL, Vold RR. 1980. Multiple quantum spin-echo spectroscopy. *J Magn Reson 37*:93–106.

Bradford MM. 1976. A rapid and sensitive method for the quantitation of microgram quantities of protein utilizing the principle of protein-dye binding. *Anal Biochem 72*:248–254.

Cho H, Krishnaraj R, Kitas E, Bannwarth W, Walsh CT, Anderson KS. 1992. Isolation and structural elucidation of a novel phosphocysteine intermediate in the LAR protein tyrosine phosphatase enzymatic pathway. *J Am Chem Soc 114*:7296–7298.

Clubb RT, Thanabal V, Wagner G. 1992. A constant-time 3-dimensional triple-resonance pulse scheme to correlate intraresidue proton ($^{1}HN$), nitrogen-15 and carbon-13 (13′) chemical shifts in nitrogen-15–carbon-13 labeled protons. *J Magn Reson 97*:213–217.

Dijkstra K, Kroon GJA, van Nuland NAJ, Scheek RM. 1994. The COCAH experiment to correlate intra-residue carbonyl, Cα and Hα resonances in proteins. *J Magn Reson*. In press.

Fesik SW, Zuiderweg ERP. 1988. Heteronuclear three-dimensional NMR spectroscopy. A strategy for the simplification of homonuclear two-dimensional NMR spectra. *J Magn Reson 78*:588–593.

Fesik SW, Zuiderweg ERP. 1990. Heteronuclear three-dimensional NMR spectroscopy of isotopically labeled macromolecules. *Q Rev Biophys 23*:97–131.

Griesinger C, Otting G, Wüthrich K, Ernst RR. 1988. Clean-TOCSY for $^{1}H$ spin system identification in macromolecules. *J Am Chem Soc 110*: 7870–7872.

Grzesiek S, Bax A. 1992. Improved 3D triple-resonance NMR techniques applied to a 31 kDa protein. *J Magn Reson 96*:432–440.

Guan K, Dixon JE. 1991. Evidence for protein-tyrosine-phosphatase catalysis proceeding via a cysteine-phosphate intermediate. *J Biol Chem 266*:17026–17030.

Howarth OW, Lilley DMJ. 1978. Carbon-13-NMR of peptides and proteins. *Progr NMR Spectrosc 12*:1–40.

Kay LE, Ikura M, Tschudin R, Bax A. 1990. Three-dimensional triple-resonance NMR spectroscopy of isotopically enriched proteins. *J Magn Reson 89*:469–514.

Kroon GJA, Grötzinger J, Dijkstra K, Scheek RM, Robillard GT. 1993. Backbone assignments and secondary structure of the *Escherichia coli* enzyme-II mannitol A domain determined by heteronuclear three-dimensional NMR spectroscopy. *Protein Sci 2*:1331–1341.

Laemmli UK. 1970. Cleavage of structural proteins during the assembly of the head of bacteriophage T4. *Nature 227*:680–685.

Lai X, Ingram LO. 1993. Cloning and sequencing of a cellobiose phosphotransferase system operon from *Bacillus stearothermophilus* XL-65-6 and functional expression in *E. coli*. *J Bacteriol 175*:6441–6450.

Lee CA, Saier MH Jr. 1983. The mannitol-specific enzyme II of the bacterial phosphotransferase system III. The nucleotide sequence of the permease gene. *J Biol Chem 285*:10761–10767.

Live DH, Davis DG, Agosta WC, Cowburn D. 1984. Long range hydrogen bond mediated effects in peptides: $^{15}N$ NMR study of gramicidin S in water and organic solvents. *J Am Chem Soc 106*:1939–1941.

Lolkema JS, Robillard GT. 1992. The enzymes II of the phosphoenolpyruvate-dependent carbohydrate transport systems. In: de Pont JJHMM, ed. *The new comprehensive biochemistry: Pumps, carriers and channels*. Amsterdam: Elsevier/North Holland Biomedical Press. pp 135–167.

Marion D, Driscoll PC, Kay LE, Wingfield PT, Bax A, Gronenborn AM, Clore GM. 1989a. Overcoming the overlap problem in the assignment of $^{1}H$-NMR spectra of larger proteins by use of three-dimensional heteronuclear $^{1}H$-$^{15}N$ Hartmann–Hahn multiple quantum coherence and nuclear-Overhauser multiple quantum coherence spectroscopy: Application to interleukin 1β. *Biochemistry 28*:6150–6156.

Marion D, Ikura M, Tschudin R, Bax A. 1989b. Rapid recording of 2D spectra without phase cycling. Application to the study of hydrogen exchange in proteins. *J Magn Reson 85*:393–399.

Marion D, Wüthrich K. 1983. Application of phase sensitive two-dimensional spectroscopy (COSY) for measurements of $^{1}H$-$^{1}H$ spin-spin coupling constants in proteins. *Biochem Biophys Res Commun 113*:967–974.

Meadow ND, Fox DK, Roseman S. 1990. The bacterial phosphoenolpyruvate: glucose phosphotransferase system. *Annu Rev Biochem 59*:497–542.

Meins M, Jenö P, Müller D, Richter WJ, Rosenbusch JP, Erni B. 1993. Cysteine phosphorylation of the glucose transporter of *E. coli*. *J Biol Chem 268*:11604–11609.

Messerle BA, Wider G, Otting G, Weber C, Wüthrich K. 1989. Solvent suppression using a spin lock in 2D and 3D NMR spectroscopy with $H_2O$ solutions. *J Magn Reson 85*:608–613.

Nakamaye KL, Eckstein F. 1986. Inhibition of restriction endonuclease NciI, cleavage by phosphorothioate groups and its application to oligonucleotide-directed mutagenesis. *Nucleic Acids Res 14*:9679–9698.

Norwood TJ, Boyd J, Heritage JE, Soffer N, Campbell ID. 1990. Comparison of techniques for $^{1}H$ detected heteronuclear $^{1}H$-$^{15}N$ spectroscopy. *J Magn Reson 87*:488–501.

Parker LL, Hall BG. 1990. Characterization and nucleotide sequence of the cryptic cel operon of *Escherichia coli* K12. *Genetics 124*:455–471.

Pas HH, Meyer G, Kruizinga WH, Tamminga KS, Van Weeghel RP, Robillard GT. 1991. $^{31}P$ phospho-NMR demonstration of phosphocysteine as a catalytic intermediate on the *Escherichia coli* phosphotransferase system $EII^{mtl}$. *J Biol Chem 266*:6690–6692.

Pas HH, Robillard GT. 1988. *S*-phosphocysteine and phosphohistidine are intermediates in the phosphoenol-pyruvate dependent mannitol transport catalyzed by *Escherichia coli* $EII^{mtl}$. *Biochemistry 27*:5835–5839.

Pas HH, Ten Hoeve-Duurkens RH, Robillard GT. 1988. Bacterial phosphoenolpyruvate dependent phosphotransferase system: Mannitol-specific EII contains two phosphoryl binding sites per monomer and one high-affinity mannitol binding site per dimer. *Biochemistry 27*:5520–5525.

Postma PW, Lengeler JW, Jacobson GR. 1993. Phosphoenolpyruvate-carbohydrate phosphotransferase systems of bacteria. *Microbiol Rev 57*:543–574.

Reizer J, Reizer A, Saier MH Jr. 1990. The cellobiose permease of *Escherichia coli* consists of three proteins and is homologous to the lactose permease of *Staphylococcus aureus*. *Res Microbiol 141*:1061–1067.

Robillard GT, Boer H, van Weeghel RP, Wolters G, Dijkstra A. 1993. Expression and characterization of a structural and functional domain of the mannitol-specific transport protein involved in the coupling of mannitol transport and phosphorylation in the phosphoenolpyruvate-dependent phosphotransferase system of *Escherichia coli*. *Biochemistry 32*:9553–9562.

Saier MH, Reizer J. 1992. Proposed uniform nomenclature for the proteins and protein domains of the bacterial phosphoenolpyruvate:sugar phosphotransferase system. *J Bacteriol 174*:1433–1438.

Sambrook J, Fritsch EF, Maniatis T. 1989. *Molecular cloning, a laboratory manual, 2nd ed*. Cold Spring Harbor, New York: Cold Spring Harbor Laboratory Press.

Shaka AJ, Barker PB, Freeman R. 1985. Computer optimized decoupling scheme for wideband applications and low level operation. *J Magn Reson 64*:547–552.

Shaka AJ, Keeler J, Freeman R. 1983. Evaluation of a new broadband decoupling sequence: WALTZ-16. *J Magn Reson 53*:313–340.

Spera S, Bax A. 1991. Empirical correlation between protein backbone conformation and Cα and Cβ $^{13}C$ nuclear magnetic resonance chemical shifts. *J Am Chem Soc 113*:5490–5492.

Wishart DS, Sykes BD, Richards FM. 1992. The chemical shift index: A fast and simple method for the assignment of protein secondary structure through NMR spectroscopy. *Biochemistry 31*:1647–1651.

Wüthrich K. 1986. *NMR of proteins and nucleic acids*. New York: Wiley. pp 117–167.

Zuiderweg ERP, Fesik SW. 1989. Heteronuclear three-dimensional NMR-spectroscopy of the inflammatory protein C5a. *Biochemistry 28*:2387–2391.